International Journal of Thermophysics, Vol. 22, No. 2, 2001

Speed of Sound of *n*-Hexane and *n*-Hexadecane at Temperatures Between 298 and 373 K and Pressures up to 100 MPa[1]

S. J. Ball[2, 3] and J. P. M. Trusler[2]

Measurements of the speed of sound u for *n*-hexane and *n*-hexadecane at temperatures of 298.3, 323.15, 348.15, and 373.15 K and at pressures up to 100 MPa are reported. The speeds of sound, the temperatures, and the pressures are subject to an uncertainty of $\pm 0.1\%$, ± 0.01 K, and ± 0.2 MPa, respectively. These measurements were undertaken using a new apparatus which has been constructed for measurement of the speed of sound in liquids and supercritical fluids at pressures up to 200 MPa and at temperatures between 248 and 473 K. The technique is based on a pulse-echo method with a single transducer placed between two plane parallel reflectors. The speed of sound is obtained from the difference between the round-trip transit times in the two paths. It is expected that both the precision and the accuracy of the method can be further improved.

KEY WORDS: acoustic; hexadecane; hexane; pulse-echo method; speed of sound.

1. INTRODUCTION

Knowledge of the thermophysical properties of organic liquids is of great importance in various fields of science and technology. As the direct determination of properties such as density and heat capacity can be quite difficult at elevated pressures, an indirect technique may have advantages. One such technique is an acoustic method in which the speed of sound u of the liquid, measured as a function of both temperature T and pressure P, is combined with direct measurements of density and heat capacity along

[1] Paper presented at the Fourteenth Symposium on Thermophysical Properties, June 25–30, 2000, Boulder, Colorado, U.S.A.

[2] Department of Chemical Engineering and Chemical Technology, Imperial College of Science, Technology and Medicine, Prince Consort Road, London SW7 2BY, United Kingdom.

[3] To whom correspondence should be addressed. E-mail: s.ball@ic.ac.uk

0195-928X/01/0300-0427$19.50/0

one isobar at a low pressure. These data are then analyzed in terms of the relation

$$u^2 = \left[\left(\frac{\partial \rho}{\partial P} \right)_T - \left(\frac{T}{\rho^2 c_p} \right) \left(\frac{\partial \rho}{\partial T} \right)_P^2 \right]^{-1} \tag{1}$$

to obtain values for density ρ and specific heat capacity c_p at elevated pressures by means of a numerical integration technique. The method was first applied, using an Euler integration method, by Davis and Gordon in their study of mercury [1]; it has been improved subsequently by various workers, including Sun et al. [2]. Once u, ρ, and c_p are known for all temperatures and pressures of interest, it is possible to calculate all observable thermodynamic properties including enthalpy increments, isochoric heat capacity, and isothermal compressibility. This technique has been used increasingly in the measurement of thermodynamic properties because it has the advantages of speed, simplicity, and high accuracy [3–5].

In this paper, measurements of the speed of sound of *n*-hexane and *n*-hexadecane are reported as part of an ongoing research program to obtain accurate thermodynamic properties for a range of key organic liquids, liquid mixtures, and mixtures containing dissolved supercritical components over wide ranges of temperature and pressure. These results are important for the fundamental theory of liquid mixtures and also for the purpose of validating thermodynamic models. An important industrial application of this research is to provide thermodynamic properties for the various oil/gas mixtures, so called "live" fluids, extracted from deep oil wells at elevated temperatures and pressures.

2. EXPERIMENTAL DETAILS

2.1. Ultrasonic Cell

The cell, shown in Fig. 1, consisted of two Type 316 stainless-steel reflectors (2), a piezoceramic transducer (5) held by means of two Type 316 stainless-steel clamping disks (4), used to provide an electrical contact (6), and two spacers (3) of unequal length. These pieces were held together by three 2-mm-diameter threaded rods which pass through clearance holes located at an angle of $2\pi/3$ to each other in the clamping disks and the reflectors. A further three holes provided in each piece were used to aid filling and evacuation of the cell. The transducer (10-mm diameter, 0.4-mm thickness) used in the cell was made from lead zirconate titanate ($PbZrO_3/PbTiO_3$) plated on both faces with nickel; it was operated at its resonant frequency of 5 MHz. Since the reflectors and the clamping disks

were fabricated from stainless steel, the material used for the spacers had to be an electrical insulator. In addition, the spacers had to be manufactured to a high tolerance to ensure good alignment, and, for these reasons, fused quartz was chosen. The hollow cylindrical spacers were 20 and 30 mm in length and had inside and outside diameters of 20 and 22 mm, respectively. They were ground from solid pieces of fused quartz such that the diameters were accurate to $\pm 10\ \mu$m, and the ends were flat and parallel to better than $\pm 2.5\ \mu$m. An advantage of using fused quartz is that its thermal expansion

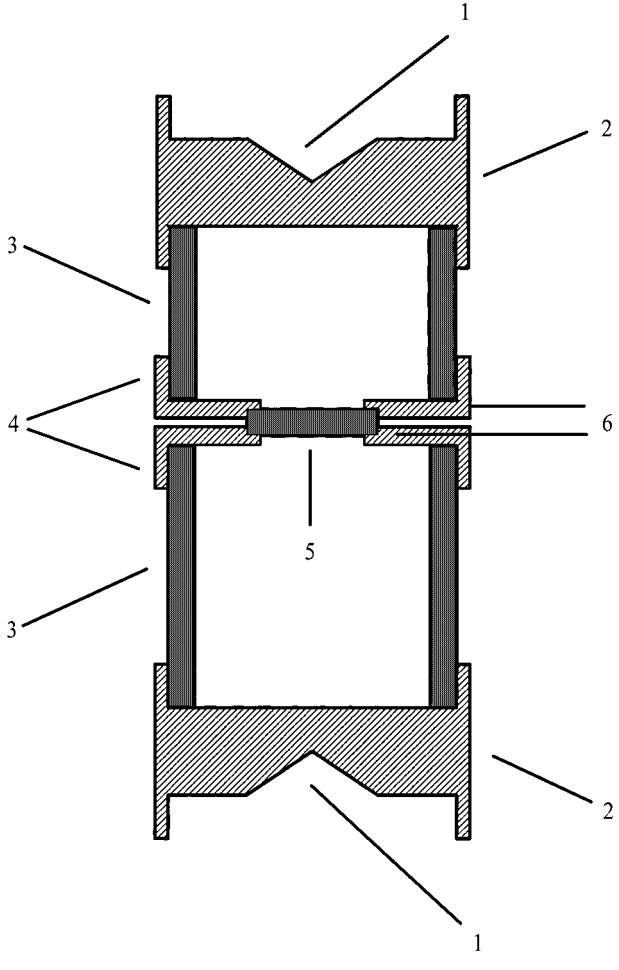

Fig. 1. Ultrasonic cell: 1, conical cavity; 2, reflectors; 3, quartz spacers; 4, clamping discs; 5, transducer; 6, electrical connections.

coefficient is very small so that corrections required to the pathlengths as the temperature was changed were minimized. The expansion and compressibility of stainless steel are also well known and were used to correct that part of the pathlength associated with the transducer clamping disks. A further feature of the cell was that the reflectors, which were 10 mm deep and 25 mm in diameter, each contained a 90° conical cavity in their rear face. The reason for this cavity was to disperse sound that passed into the reflector and then re-reflected back into the cell, possibly causing erroneous results.

The chosen dimensions of the cell and the transducer were determined from an analysis of signal diffraction which is present in all pulse measurements. To ensure that the cavity walls do not affect the acoustic signal as it passes through the fluid, it is important that the cavity is significantly greater in diameter than the source. This problem was analyzed by calculating the steady-state radiation pattern from the source and choosing a cell diameter such that an insignificant fraction of the acoustic energy impinged on the walls. A second effect of the signal diffraction is that it causes the measured transit time to be in error, because of a phase advance ϕ of the sound wave relative to a plane wave passing through the same distance [7]. To correct for this error, the transit time must be increased by an increment δt, given by

$$\delta t = \frac{\phi(L)}{2\pi f} \tag{2}$$

where f is the frequency of the source, L is the pathlength, and ϕ is the phase advance calculated, either numerically or analytically, from the free-field diffraction equation:

$$A \exp(i\phi) = 1 - \frac{4}{\pi} \int_0^{\pi/2} \exp\left[-\left(\frac{4b^2 \pi i}{L\lambda} \right) \cos^2 \theta \right] \sin^2 \theta \, d\theta \tag{3}$$

with b representing the radius of the source. It was found that with the double-path configuration and the chosen dimensions, this correction amounted to less than 0.01 % of the measured transit time difference.

2.2. Methodology

The transducer was energized with a single five-cycle tone burst at 5 MHz with an amplitude of 10 V peak to peak. This caused the transducer to emit acoustic pulses simultaneously in opposite directions. The signal

across the transducer was digitised at a sampling rate of 200 MHz by a digital storage oscilloscope. A typical trace is shown in Fig. 2. In Trace 1 the burst on the left represents the excitation signal from the function generator and the other two bursts represent the first echoes returning from the two reflectors. Trace 2 shows the two echoes in more details, and an important feature to note is the essentially identical shape of the two returning bursts.

Let the time at which a characteristic feature (such as the leading edge or the maximum amplitude) of the first echo returning on the shorter path L_1 was detected be t_1. Similarly, let the time at which the first echo returning on the longer path L_2 was detected be t_2. Then, ignoring diffraction corrections, the speed of sound is obtained as

$$u = \frac{2\Delta L}{\Delta t} \tag{4}$$

where $\Delta L = (L_2 - L_1)$ and $\Delta t = (t_2 - t_1)$. As mentioned previously, an advantage of this method is that, by calculating the difference in the transit times, errors such as diffraction and electronic delays, can be reduced or eliminated. Times may be read from the oscilloscope with a resolution of 10 ns. However, the resolution of this method is further improved by applying the following numerical analysis. The data, which are given as voltages V digitized with 8-bit resolution every 5 ns with 40-ps timing accuracy, were first downloaded to a computer for analysis. A section of the record, typically 10 cycles, relating to the first echo was then identified and cut out. By assuming a time delay Δt, a second cut was made from the record, again typically of 10 cycles' duration, and then the data from both sections were fitted to the following equation by means of a least-squares analysis:

$$V_1(t_i) = A V_2(t_i + \Delta t) \tag{5}$$

Here V_1 relates to the data from the first cut, V_2 relates to the data from the second cut, and A is an amplitude factor which is required to account for the fact that the second reflection suffers from a greater attenuation than the first. The optimum value of A corresponding to an assumed Δt is obtained from the expression,

$$A = \frac{\sum_i V_1(t_i)\, V_2(t_i + \Delta t)}{\sum_i V_2^2(t_i + \Delta t)} \tag{6}$$

Trace 1

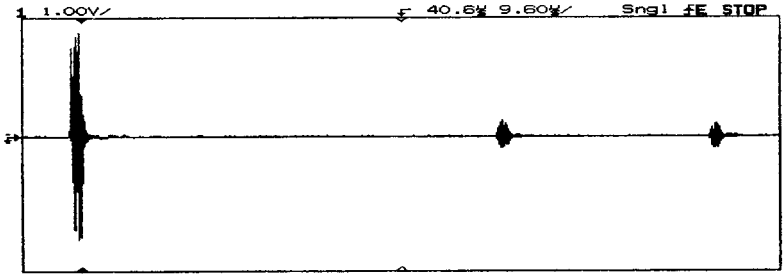

Trace 2

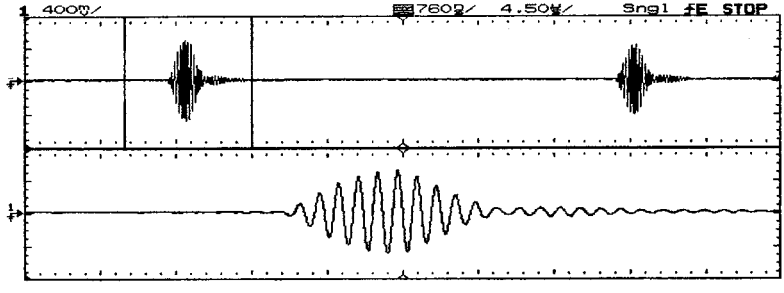

Trace 3

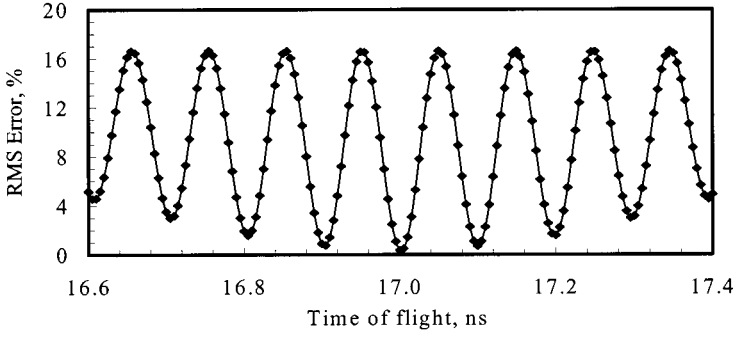

Fig. 2. Oscilloscope traces.

The analysis was repeated for various trial values of Δt, rounded to the nearest 5 ns, and, for each trial, α^2 was calculated, where

$$\alpha^2 = \sum_i [\, V_1(t_i) - V_2(t_i + \Delta t)]^2 \tag{7}$$

The results are shown in Fig. 2, Trace 3. As can be seen, the fitting error is very small, and this is a consequence of both echoes being essentially identical in shape as mentioned previously. A number of discrete data points located around the global minima were then fitted by a parabolic equation,

$$\alpha^2 = x(\Delta t)^2 + y(\Delta t) + z \tag{8}$$

where x, y, and z represent the polynomial coefficients, and the minimum found. This leads to the optimum transit time Δt. To check the precision of this analysis, it was determined by how much the transit time would need to change in order to double α^2, and it was found that the transit time changed by less than the timing accuracy of the oscilloscope (± 40 ps). Repeated measurements at the same state point were found to be reproducible to within $\pm 0.002\%$.

The pathlength difference ΔL was calibrated at a reference point ($T^0 = 298$ K, $P^0 = 0.1$ MPa) by means of measurements with water using Del Grosso's [8] value for the speed of sound. The variation of ΔL with temperature T and pressure P was calculated from the formula

$$\begin{aligned}\Delta L(T, P) = {} & \Delta L_Q(T^0, P^0)[(1 + \alpha_Q \Delta T + \beta_Q \Delta P) - (1 + \alpha_{SS} \Delta T + \beta_{SS} \Delta P)] \\ & + \Delta L(T^0, P^0)(1 + \alpha_{SS} \Delta T + \beta_{SS} \Delta P)\end{aligned} \tag{9}$$

where α and β [9], the coefficients of thermal expansion and compressibility, respectively, of the quartz (Q) and stainless steel (SS), are assumed to be independent of temperature. The temperatures and pressures differing from the reference state are represented as ΔT and ΔP, respectively. The magnitudes of the corrections required for the pathlength are 0.18% at the maximum pressure (200 MPa) and 0.012% at the maximum temperature (473 K).

2.3. Pressure System

The acoustic cell described in Section 2.1 was contained within a pressure vessel, made from a nickel–chromium alloy (Nimonic 80A, Henry Wiggin Ltd.), which has been specifically designed and fabricated for this

research. It is pressure rated for 200 MPa. The pressure vessel, illustrated in Fig. 3, is based on a standard design incorporating a Viton o-ring (4) and a phosphor bronze antiextrusion ring (3). The force to compress the o-ring and create a seal is supplied by a combination of the screw cap and the eight high-tensile steel bolts. Due to the small size of the acoustic cell, the pressure vessel was, in turn, designed to be as compact as possible. The approximate dimensions are an overall length of 175 mm, a body diameter of 50 mm, and an internal volume of approximately 50 cm^3. The vessel has one entry port (1) in the lid, which was used for two purposes. The first was for filling the system, and the second was as a means of entry for the

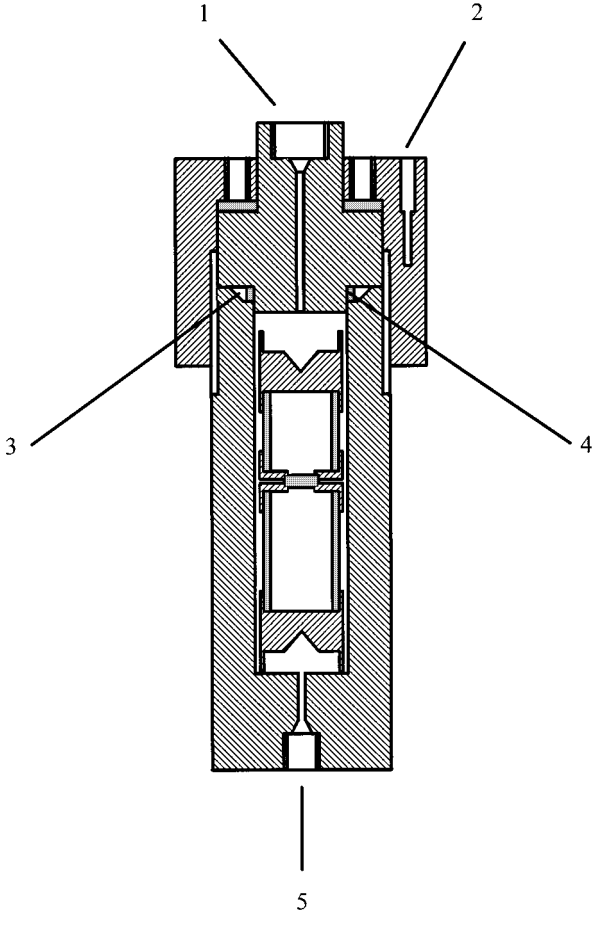

Fig. 3. Pressure vessel: 1, liquid inlet; 2, PRT well; 3, anti-extrusion ring; 4, Viton o-ring; 5, liquid outlet.

wiring used to power the transducer in the acoustic cell. The point where the wire leaves the high pressure system was sealed with epoxy resin so that it was pressure- and leak-tight. A second port (5) located in the base of the vessel was used to empty the vessel when required. A well was also provided in the cap of the pressure vessel (2) for a platinum resistance thermometer.

Other equipment in the system included a 200-MPa pressure intensifier of 12-cm^3 capacity, a two-stage vacuum pump, and a compressed-gas line. A pressure transducer (Paroscientific Model 440K) was used to measure the pressure in the system with an uncertainty of ± 0.2 MPa. It was calibrated over its full operating range (273 to 323 K and 0 to 200 MPa) against a Barnet Instruments oil operated deadweight tester. An analogue gauge, calibrated for pressures up to 300 MPa, was also included. A further feature of the pressure system was that it was contained within an insulated enclosure which allowed the components to be thermostated at above-ambient temperatures when required, to avoid freezing of the liquid under study. The transfer line from the pressure system to the pressure vessel also had the facility to be heated when required.

2.4. Temperature Control

The ultrasonic cell and pressure vessel were thermostated in a custom-built bath which was based on a standard glass Dewar vessel with a capacity of approximately 6.5 dm^3. Heat loss through the lid was further reduced by the use of silicone rubber insulation. A narrow vertical strip of the Dewar wall was left unsilvered for viewing purposes (for example, to monitor the level of the bath fluid, which changed due to thermal expansion over the temperature range). A facility was also included for the addition and removal of bath fluid as required to compensate for this thermal expansion. The bath fluid used was a silicone oil (Dow Corning 200/10) which could be used over the entire temperature range (248 to 473 K). The mechanism for the fluid circulation was provided by a stirrer and a baffle within the bath. Temperature control was maintained by a proportional-integral-derivative temperature controller operating with a platinum resistance probe and a 100-W control heater. For the low-temperature investigations, a refrigeration unit was used with a heat exchange coil which could be removed from the bath when not required. Both the cooling coil and the heaters were located close to the stirrer to aid thermal equilibrium in the bath. Two further platinum resistance thermometers were used to check uniformity of temperature throughout the bath. All of the thermometers were calibrated to an accuracy of ± 10 mK by means of comparison with

Table I. Experimental Values of the Speed of Sound u for *n*-Hexane as a Function of Temperature and Pressure

P (MPa)	u ($m \cdot s^{-1}$)	P (MPa)	u ($m \cdot s^{-1}$)	P (MPa)	u ($m \cdot s^{-1}$)
		$T = 298.3$ K			
0.100	1085.68	35.660	1312.19	70.871	1485.33
5.385	1122.19	40.251	1337.46	75.516	1504.29
10.560	1158.99	45.846	1367.12	80.669	1526.33
15.392	1191.50	50.507	1390.39	85.040	1543.77
20.605	1224.52	55.993	1416.99	90.837	1564.88
25.917	1256.05	60.797	1439.72	95.399	1581.45
30.468	1282.77	65.226	1460.73	100.604	1600.27
		$T = 323.15$ K			
0.100	971.42	35.149	1225.99	70.875	1411.77
5.499	1015.77	40.623	1258.35	75.234	1431.21
10.723	1058.53	45.946	1288.47	80.494	1454.05
15.993	1098.63	50.809	1314.34	85.371	1473.56
20.004	1128.15	55.066	1335.92	90.499	1494.11
25.267	1163.84	60.096	1360.40	95.111	1512.49
30.336	1196.29	65.211	1386.53	100.002	1531.29
		$T = 348.15$ K			
5.672	923.00	40.604	1179.37	75.174	1366.18
10.045	959.78	45.385	1208.26	80.399	1388.83
15.948	1008.87	50.102	1235.82	85.507	1411.90
20.114	1040.50	55.699	1267.06	90.500	1431.50
25.367	1078.74	60.318	1292.27	95.626	1452.67
30.283	1113.84	65.299	1317.88	100.388	1470.11
35.884	1149.49	70.002	1340.42		
		$T = 373.15$ K			
5.009	817.15	40.781	1109.58	75.227	1303.72
10.264	868.62	45.205	1138.88	80.184	1326.66
15.040	912.98	50.633	1170.85	85.361	1350.30
20.344	959.01	55.006	1196.25	90.956	1375.90
25.926	1004.23	60.715	1228.73	95.047	1392.48
30.599	1038.85	65.992	1256.33	100.965	1418.76
35.371	1073.13	70.348	1278.10		

a standard platinum resistance thermometer previously calibrated on the ITS-90 temperature scale by the U.K. National Physics Laboratory.

2.5. Materials

The materials used in this study, *n*-hexane and *n*-hexadecane, were supplied by Sigma–Aldrich Ltd. Both had a specified minimum purity of 99%, by volume, and the *n*-hexadecane was also anhydrous. Both were used without any further purification.

Table II. Experimental Values of the Speed of Sound u for *n*-Hexadecane as a Function of Temperature and Pressure

P (MPa)	u ($m \cdot s^{-1}$)	P (MPa)	u ($m \cdot s^{-1}$)	P (MPa)	u ($m \cdot s^{-1}$)
		$T = 298.3$ K			
0.100	1339.22	10.665	1395.14	20.772	1444.64
5.315	1367.08	15.478	1418.93	25.387	1466.41
		$T = 323.15$ K			
0.100	1248.11	30.642	1411.64	60.274	1538.62
5.385	1278.25	35.721	1435.51	65.618	1557.88
11.083	1310.66	40.452	1457.12	70.045	1573.13
15.721	1335.90	45.039	1477.22	75.832	1592.19
20.956	1363.27	50.147	1498.54	80.126	1605.64
26.086	1389.62	55.991	1522.07		
		$T = 348.15$ K			
0.100	1160.59	35.526	1363.56	70.555	1507.35
5.639	1195.53	40.115	1385.67	75.235	1523.80
10.994	1228.64	45.345	1409.64	80.669	1540.16
15.238	1253.96	50.821	1433.32	85.204	1553.81
20.459	1283.99	55.923	1454.06	90.499	1566.05
25.008	1309.13	60.381	1471.12	95.173	1576.63
30.294	1337.14	65.941	1492.02	100.883	1586.75
		$T = 373.15$ K			
0.100	1074.99	35.995	1301.00	70.359	1445.03
5.329	1113.56	40.420	1323.57	75.111	1459.82
10.618	1149.52	45.614	1348.26	80.985	1478.43
15.692	1181.62	50.992	1373.33	85.304	1488.98
20.045	1208.94	55.561	1392.53	90.275	1501.21
25.727	1243.88	60.887	1411.89	95.222	1511.23
30.462	1269.44	65.193	1427.98	100.845	1522.14

3. RESULTS

The experimental values of the speed of sound u for n-hexane and n-hexadecane at 150 points are listed in Tables I and II, respectively. These measurements were carried out on four isotherms, at $T = 298.3$, 323.15, 348.15, and 373.15 K, and in approximately 5-MPa pressure increments from atmospheric pressure to 100 MPa. As the apparatus used in this study is suitable only for the study of liquids, some temperature and pressure combinations were not possible for the liquids under investigation. This is shown for n-hexane, where low-pressure readings at 348.15 and 373.15 K were not taken due to the sample being in the vapor state, and for n-hexadecane, where, at pressures above 25 MPa at 298.13 K and above 80 MPa at 323.15 K, freezing occurs. Data relating to the freezing pressure of n-hexadecane were given by Tanaka et al. [10].

The data, which are shown graphically in Figs. 4 and 5, have been fitted by the following polynomial for each isotherm:

$$u = a_0 + a_1 P + a_2 P^2 + a_3 P^3 \tag{10}$$

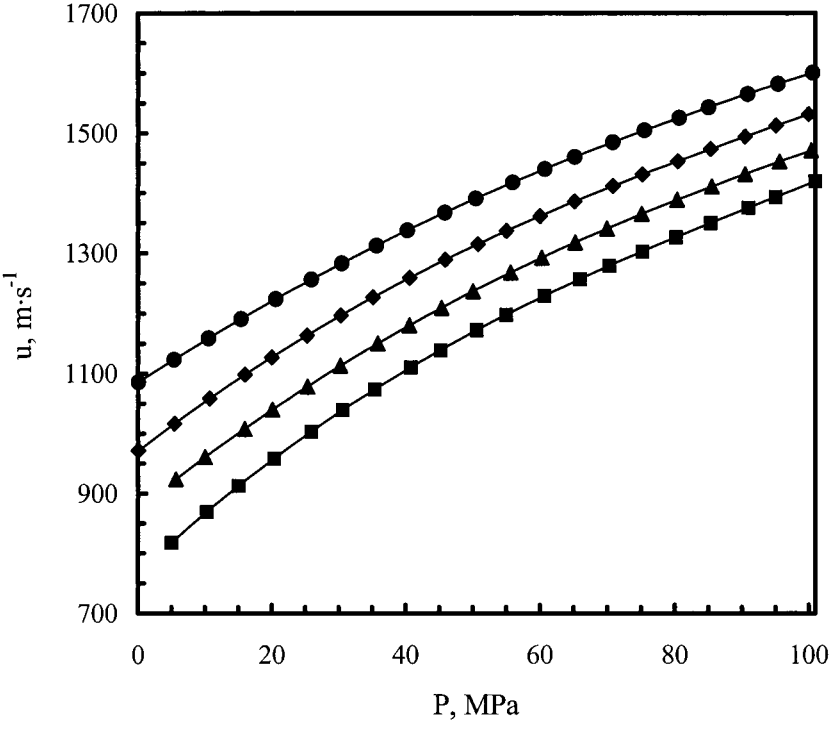

Fig. 4. Speed of sound u of n-hexane as a function of pressure. (●) $T = 298.3$ K; (◆) $T = 323.15$ K; (▲) $T = 348.15$ K; (■) $T = 373.15$ K.

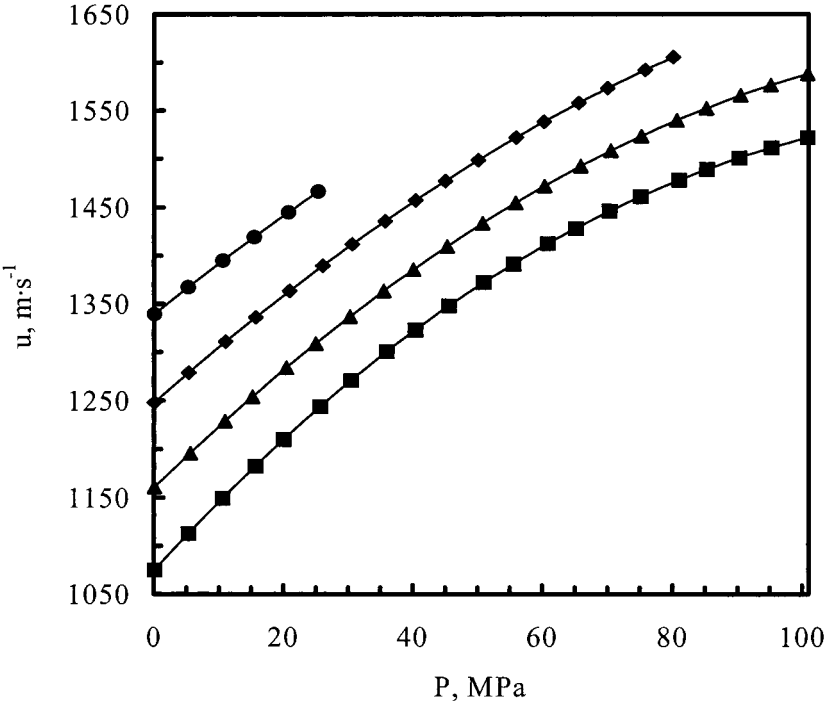

Fig. 5. Speed of sound u of *n*-hexadecane as a function of pressure. (●) $T = 298.3$ K; (◆) $T = 323.15$ K; (▲) $T = 348.15$ K; (■) $T = 373.15$ K.

with the polynomial coefficients listed in Table III. To check the consistency of the fits, the deviations at each experimental point for both *n*-hexane and *n*-hexadecane were calculated with the results for *n*-hexadecane shown in Fig. 6. This gave a maximum deviation of 0.1%. However, it can be seen from the graph that this deviation increases with temperature and that, for the 323.15 K isotherm, the deviations are typically less than 0.02%. We suspect that the increased scatter at higher temperatures may have been caused by differential thermal expansion of the components, leading to loss of tension in the threaded rods holding the cell together. In view of this problem, we associate the speeds of sound with an uncertainty of $\pm 0.1\%$. We also recall that temperatures are subject to an uncertainty of ± 0.01 K and pressures are subject to an uncertainty of ± 0.2 MPa.

We have compared our results with data reported by other authors. For *n*-hexane, our data were compared to the results of Daridon et al. [3]. As shown in Fig. 7, it was found that their results typically deviated by $\pm 0.3\%$ with the values calculated from Eq. (10), with a maximum deviation

Table III. Polynomial Coefficients of Eq. (10) and Standard Deviations

T (K)	a_0	a_1	a_2	a_3	σ (m·s^{-1})
			n-hexane		
298.30	1084.95240	7.2539168	−0.0263343	5.1314E-05	0.52
323.15	970.55706	8.6394928	−0.0433947	1.3114E-04	0.57
348.15	873.67423	9.0523877	−0.0413296	1.0416E-04	0.76
373.15	766.29136	10.5989150	−0.0613684	2.0254E-04	0.69
			n-hexadecane		
298.30	1338.67240	5.4503156	−0.0165922		0.15
323.15	1247.52480	5.9037102	−0.0178622	−6.8518E-07	0.19
348.15	1159.94010	6.4964959	−0.0214881	−8.4625E-06	0.62
373.15	1074.24700	7.3888749	−0.0314846	2.2073E-05	0.76

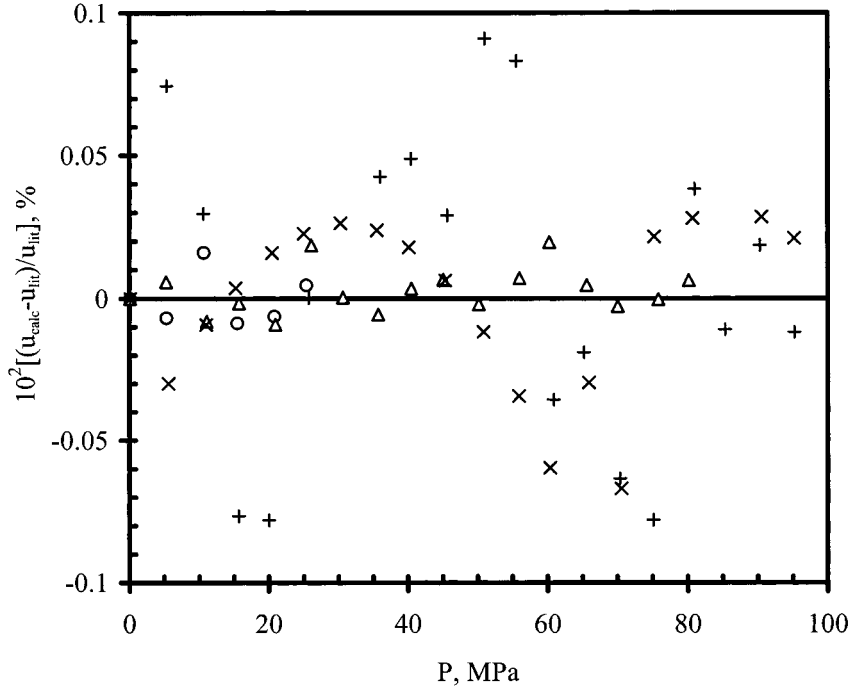

Fig. 6. Deviations from Eq. (10) for *n*-hexadecane. (○) $T = 298.3$ K; (△) $T = 323.15$ K; (×) $T = 348.15$ K; (+) $T = 373.15$ K.

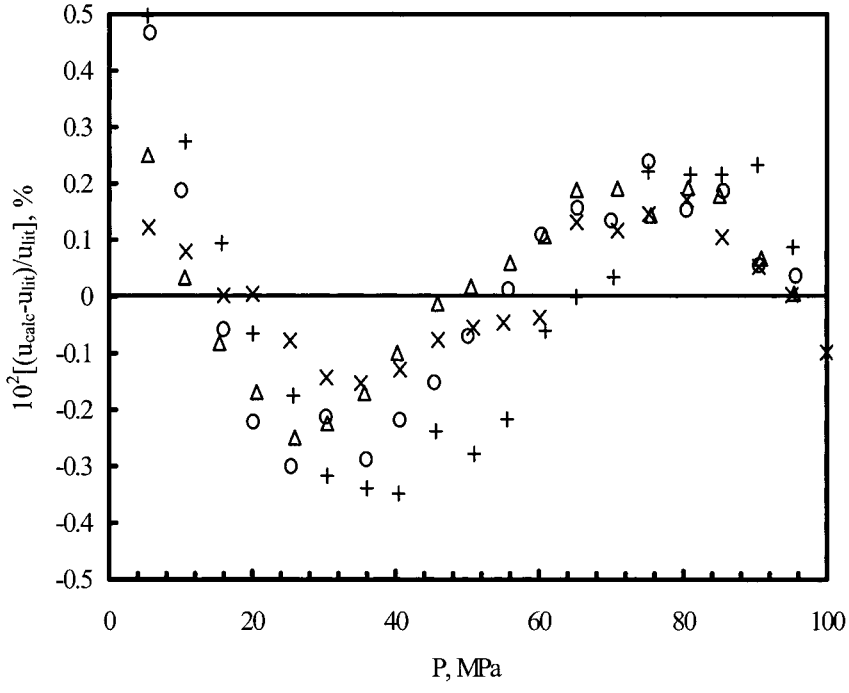

Fig. 7. Deviations of the Daridon et al. [3] data for the speed of sound of *n*-hexane from Eq. (10). (△) $T = 298.3$ K; (×) $T = 323.15$ K; (○) $T = 348.15$ K; (+) $T = 373.15$ K.

of 0.5% at the lowest pressures. Daridon et al. also compared their data to the results of other authors and reported good agreement with Boelhouwer [11], but compared with other sources [12, 13], deviations of 0.79 and 0.81% were noted. For *n*-hexadecane there are only limited data available. The deviations of the results of Ye et al. [14] and of Boelhouwer [11], as shown in Fig. 8, are typically ± 0.2 and ± 0.3%, respectively.

4. CONCLUSIONS

Speeds of sound are presented for *n*-hexane and *n*-hexadecane at temperatures between 298 and 373 K and at pressures up to 100 MPa. These results show an internal consistency of 0.1% and are also in agreement with other authors to within 0.5%. The new apparatus described in this paper provides a fast and accurate method for obtaining the speed of sound over a wide range of temperature and pressure. These results form a small part of an ongoing research program to obtain accurate thermodynamic properties for a range of key organic liquids, their mixtures, and "live"

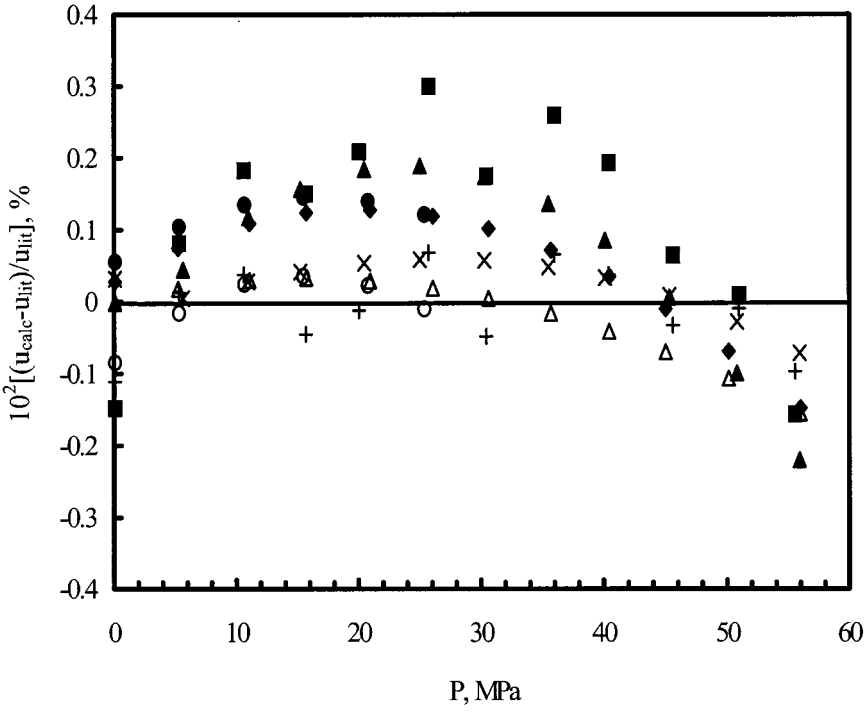

Fig. 8. Deviations of literature data for the speed of sound of *n*-hexadecane from Eq. (10). Boelhower [11] data: (●) $T = 298.3$ K; (◆) $T = 323.15$ K; (▲) $T = 348.15$ K; (■) $T = 373.15$ K. Ye et al. [12] data: (△) $T = 298.3$ K; (×) $T = 323.15$ K; (○) $T = 348.15$ K; (+) $T = 373.15$ K.

fluids from a combination of speed-of-sound, density, and heat capacity data. Future publications will report a more detailed analysis of the results.

We believe that the precision and accuracy of the results could be improved by (a) an improved method of holding the cell components firmly together and (b) increased accuracy in the measurement of pressure.

ACKNOWLEDGMENT

The authors wish to acknowledge the financial support from the United Kingdom Engineering and Physical Sciences Research Council.

REFERENCES

1. L. A. Davis and R. B. Gordon, *J. Chem. Phys.* **46**:2650 (1967).
2. M. J. P. Muringer, N. J. Trappeniers, and S. N. Biswas, *Phys. Chem. Liq.* **14**:273 (1985).

3. J. Daridon, B. Lagourette, and J. Grolier, *Int. J. Thermophys.* **19**:145 (1998).
4. T. F. Sun, P. J. Kortbeek, N. J. Trappeniers, and S. N. Biswas, *Phys. Chem. Liq.* **16**:163 (1987).
5. J. P. Petitet, R. Tufeu, and B. Le Neindre, *Int. J. Thermophys.* **4**:35 (1983).
7. A. O. Williams, *J. Acoust. Soc. Am.* **23**:1 (1951).
8. V. A. Del Grosso, *J. Acoust. Soc. Am.* **47**:947 (1969).
9. G. W. C. Kaye, *Tables of Physical and Chemical Constants* (Longman, London, 1986).
10. Y. Tanaka and M. Kawakami, *Fluid Phase Equil.* **125**:103 (1996).
11. J. Boelhouwer, *Physica* **34**:484 (1967).
12. B. S. Kiryakov and P. P. Panin, *Nauk. Tr. Kursk. Gos Pedagog. Inst.* **7**:132 (1972).
13. L. S. Kagramanyan and A. L. Badalyan, *Izv. Akad. Nauk. Arm. USSR Fiz.* **13**:478 (1978).
14. S. Ye, J. Alliez, B. Lagourette, H. Saint-Guirons, J. Arman, and P. Xans, *Rev. Phys. Appl.* **25**:555 (1990).